Time delay in XUV/IR photoionization of H_2O

Vladislav V. Serov, and Anatoli S. Kheifets

Citation: The Journal of Chemical Physics **147**, 204303 (2017); doi: 10.1063/1.4993493
View online: https://doi.org/10.1063/1.4993493
View Table of Contents: http://aip.scitation.org/toc/jcp/147/20
Published by the American Institute of Physics

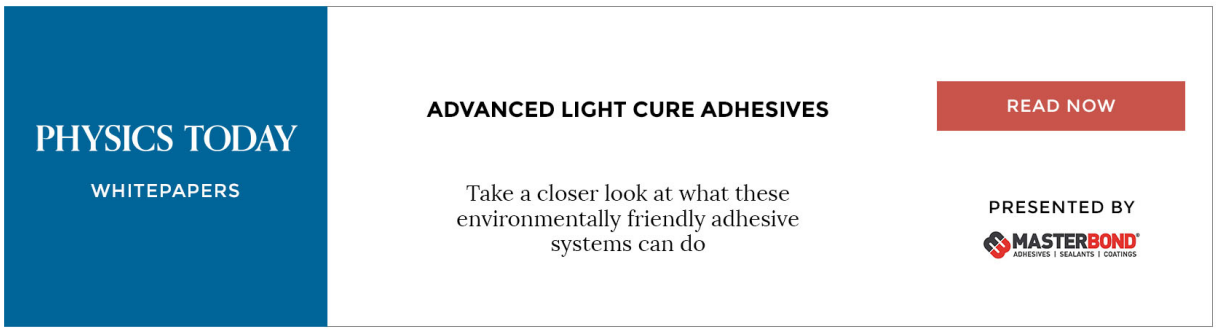

Time delay in XUV/IR photoionization of H_2O

Vladislav V. Serov[1] and Anatoli S. Kheifets[2]
[1]*Department of Theoretical Physics, Saratov State University, 83 Astrakhanskaya, Saratov 410012, Russia*
[2]*Research School of Physics and Engineering, The Australian National University, Canberra ACT 2601, Australia*

(Received 29 June 2017; accepted 9 November 2017; published online 29 November 2017)

We solve the time-dependent Schrödinger equation describing a water molecule driven by a superposition of the extreme ultraviolet and IR pulses typical for a reconstruction of attosecond beating by interference of two-photon transitions experiment. This solution is obtained by a combination of the time-dependent coordinate scaling and the density functional theory with self-interaction correction. Results of this solution are used to determine the time delay in photoionization of the water and hydrogen molecules. *Published by AIP Publishing.* https://doi.org/10.1063/1.4993493

I. INTRODUCTION

Time delay in molecular photoionization can now be measured by using the RABBITT technique (Reconstruction of Attosecond Beating By Interference of Two-photon Transitions). In the pioneering experiment, Huppert *et al.*[1] determined the relative delay in photoemission of the outer-most valence shells of the H_2O and N_2O molecules. The Eisenbud-Wigner-Smith component of the measured time delay (Wigner time delay for brevity), related to the extreme ultraviolet (XUV) photon absorption, was evaluated from the complex dipole matrix elements provided by molecular quantum scattering theory.[2] The Coulomb-laser coupling (CLC) correction, associated with the IR dressing field, was accounted for separately in an atomic-like fashion.

In the present work, we provide an alternative approach where the ionizing XUV field and the dressing IR field drive the molecular time-dependent Schrödinger equation (TDSE). This equation is solved by a combination of the time-dependent coordinate scaling (TDCS) and the density functional theory with self-interaction correction (DFT-SIC). We applied the TDCS technique in our earlier work to describe a RABBITT measurement on the molecular H_2^+ ion.[3] An advantage of this technique is that the TDSE is solved directly in the XUV and IR fields, and the calculated (and measurable) time delay is not artificially split into the Wigner and CLC components. The earlier application to H_2^+ was based on the explicit form of the one-electron potential. For more complex molecules such as H_2 and H_2O, this potential can be evaluated within the DFT-SIC approach.

II. THEORETICAL METHODS

A. Time-dependent scaling method

We restrict ourselves with a single active electron (SAE) approximation and write the TDSE as

$$i\frac{\partial\Psi(\mathbf{r},t)}{\partial t} = \hat{H}\Psi(\mathbf{r},t) \tag{1}$$

with the Hamiltonian

$$\hat{H} = \frac{\hat{p}^2}{2} - \mathbf{A}(t)\hat{\mathbf{p}} + U(\mathbf{r}). \tag{2}$$

Here $\hat{\mathbf{p}} = -i\nabla$ is the momentum operator, $U(\mathbf{r})$ is the effective potential of the interaction of an active electron with the ion remainder, and $\mathbf{A}(t)$ is the vector potential of the external electromagnetic field. The latter is defined as

$$\mathbf{A}(t) = -\int_0^t q\mathbf{E}(t')dt\,. \tag{3}$$

Here $\mathbf{E}(t)$ is the electric field vector. The atomic units are in use throughout the paper such that $e = m = \hbar = 1$. The factor $1/c$ with the speed of light $c \simeq 137$ and the electron charge $q = -1$ are absorbed into the vector potential.

In a RABBITT measurement, a target atom or molecule is subjected to an attosecond pulse train (APT) and infrared (IR) waveform . The vector potential of these two fields

$$\mathbf{A}(t) = \mathbf{A}_{\rm APT}(t) + \mathbf{A}_{\rm IR}(t-\tau), \tag{4}$$

where τ is the relative displacement of the XUV and IR pulses.

The APT field can be represented as

$$\mathbf{A}_{\rm APT}(t) = \sum_{\nu=-\lfloor N_{\rm APT}/2\rfloor}^{\lfloor N_{\rm APT}/2\rfloor} (-1)^\nu f_{\rm env}(t_\nu)\mathbf{A}_{\rm XUV}(t-t_\nu)\,, \tag{5}$$

where $N_{\rm APT}$ is the number of pulses in the APT and the arrival time of each pulse

$$t_\nu = \frac{T_{\rm IR}}{2}\nu \tag{6}$$

is a half integer of the period of the IR oscillation $T_{\rm IR} = 2\pi/\omega$. The envelope of the APT is modeled by

$$f_{\rm env}(t) = \exp\left(-2\ln 2\frac{t^2}{\tau_{\rm APT}^2}\right), \tag{7}$$

where $\tau_{\rm APT}$ is the full width at half maximum (FWHM) of train.

We model each ultrashort XUV pulse in train by the function

$$\mathbf{A}_{\mathrm{XUV}}(t) = -\mathbf{n}_{\mathrm{XUV}} A_{\mathrm{XUV}} \exp\left(-2\ln 2 \frac{t^2}{\tau_{\mathrm{XUV}}^2}\right) \cos\omega_{\mathrm{XUV}} t\,, \tag{8}$$

with the FWHM τ_{XUV} of pulse. The long-duration IR pulse is described by the continuous wave

$$\mathbf{A}_{\mathrm{IR}}(t) = -\mathbf{n}_{\mathrm{IR}} A_{\mathrm{IR}} \cos\omega t. \tag{9}$$

The vectors $\mathbf{n}_{\mathrm{XUV}}$ and $\mathbf{n}_{\mathrm{IR}}$ are polarization directions of XUV and IR fields, respectively.

As the XUV field is typically weak, we can calculate contributions of each XUV pulse to ionization, and after that summarize these contributions to get the ionization amplitude for all train.[3] Due to such split, we can assume evolution only in field single XUV pulse and IR wave,

$$\mathbf{A}(t) = \mathbf{A}_{\mathrm{XUV}}(t) + \mathbf{A}_{\mathrm{IR}}(t-\tau). \tag{10}$$

After the end of the XUV pulse, we employ an expanding coordinate system.[4] In this method, which we term the time-dependent coordinate scaling (TDCS), the following variable transformation is made:

$$\mathbf{r} = a(t)\boldsymbol{\xi}\,. \tag{11}$$

Here $a(t)$ is a scaling factor with an asymptotically linear time dependence $a(t\to\infty) = \dot{a}_\infty t$ and $\boldsymbol{\xi}$ is a coordinate vector. Such a transformation makes the coordinate frame to expand along with the wave packet. In addition, the following transformation is applied to the wave function:

$$\Psi(a(t)\boldsymbol{\xi}, t) = \frac{1}{[a(t)]^{3/2}} \exp\left(\frac{i}{2} a(t)\dot{a}(t)\xi^2\right) \psi(\boldsymbol{\xi}, t). \tag{12}$$

Such a transformation removes a rapidly oscillating phase factor from the wave function in the asymptotic region.[4] Thus the transformed wave function satisfies the equation

$$i\frac{\partial\psi(\boldsymbol{\xi},t)}{\partial t} = \left[\frac{\hat{p}_\xi^2}{2[a(t)]^2} - \frac{\mathbf{A}(t)\cdot\hat{\mathbf{p}}_\xi}{a(t)} + U[a(t)\boldsymbol{\xi}] + \frac{a(t)\ddot{a}(t)}{2}\xi^2 - \dot{a}(t)\mathbf{A}(t)\cdot\boldsymbol{\xi}\right]\psi(\boldsymbol{\xi},t), \tag{13}$$

where $\hat{\mathbf{p}}_\xi = -i\nabla_\xi = -i\left(\frac{\partial}{\partial\xi_x}, \frac{\partial}{\partial\xi_y}, \frac{\partial}{\partial\xi_z}\right)$. A remarkable property of the expanding coordinate system is that the ionization amplitude $f(\mathbf{k})$ is related with the wave function $\psi(\boldsymbol{\xi}, t)$ by a simple formula,[4]

$$|f(\mathbf{k})|^2 = \dot{a}_\infty^{-3} \lim_{t\to\infty} |\psi(\mathbf{k}/\dot{a}_\infty, t)|^2. \tag{14}$$

In practice, the evolution is traced for a very large time $t_f >> T_{\mathrm{IR}}$ and then the ionization probability density is obtained from the expression

$$P^{(3)} \equiv \frac{dP}{dk_x dk_y dk_z} = |f(\mathbf{k})|^2 \simeq \dot{a}_\infty^{-3} |\psi(\mathbf{k}/\dot{a}_\infty, t_f)|^2. \tag{15}$$

We use the piecewise linear scaling

$$a(t) = \begin{cases} 1, & t < t_1, \\ \dot{a}_\infty t, & t > t_1. \end{cases} \tag{16}$$

The expansion of the frame starts at the moment $t_1 >> \tau_{\mathrm{XUV}}$. We choose $\dot{a}_\infty = 1/t_1$. Such a choice ensures that the wave packet remains stationary in the expanding frame at $t > t_1$.

The coordinate frame (11) is well suited for approximating an expanding wave packet. However, its drawback is that the bound states are described progressively less accurately as the coordinate frame and its numerical grid expands. In our approach, bound states are suppressed after the start of coordinate system expansion by introducing an imaginary absorbing potential near the origin,

$$U_{sa}(\xi, t) = -i\frac{s(t)}{a(t)} e^{-\xi^2}. \tag{17}$$

Unlike in the previous treatment,[3] here we use a smooth switching of the imaginary absorbing potential by setting

$$s(t) = \begin{cases} 0, & t < t_1, \\ (1 + \cos[\pi(t - 2t_1)/t_1])/2, & t \in [t_1, 2t_1], \\ 1, & t > 2t_1. \end{cases} \tag{18}$$

This reduces spurious transitions from the bound states to continuum.

B. Density functional theory with self-interaction correction

We employ the density functional theory (DFT) with the self-interaction correction (SIC).[5] This correction is necessary to restore the Coulomb asymptotics of the photoelectron interaction with the residual ion which is essential for time delay calculations.

The density functional with the SIC[5] contains the Hartree $E_{\mathrm{H}}\{\rho\}$ and the exchange-correlation $E_{\mathrm{XC}}\{\rho_\uparrow, \rho_\downarrow\}$ components,

$$E_{\mathrm{SIC}} = E_{\mathrm{H}}\{\rho\} + E_{\mathrm{XC}}\{\rho_\uparrow, \rho_\downarrow\} - [E_{\mathrm{H}}\{\rho_i\} + E_{\mathrm{XC}}\{\rho_i, 0\}], \tag{19}$$

where the electron density

$$\rho(\mathbf{r}) = \sum_{i=1}^{N_e} \rho_i(\mathbf{r}) \tag{20}$$

is the sum of the particle densities of the ith electron orbital

$$\rho_i(\mathbf{r}) = |\varphi_i(\mathbf{r})|^2\,. \tag{21}$$

Here we consider only molecules with fully coupled electrons and hence the density of the spin-up and spin-down electrons are equal,

$$\rho_\uparrow(\mathbf{r}) = \rho_\downarrow(\mathbf{r}) = \rho(\mathbf{r})/2. \tag{22}$$

The Hartree energy is

$$E_{\mathrm{H}}\{\rho\} = \frac{1}{2}\iint \frac{\rho(\mathbf{r})\rho(\mathbf{r}')}{|\mathbf{r}' - \mathbf{r}|} d\mathbf{r}' d\mathbf{r}. \tag{23}$$

The exchange-correlation functional is expressed in the local density approximation (LDA),

$$E_{\mathrm{XC}}\{\rho_\uparrow, \rho_\downarrow\} = \int [\rho_\uparrow(\mathbf{r}) + \rho_\downarrow(\mathbf{r})]\varepsilon_{\mathrm{XC}}[\rho_\uparrow(\mathbf{r}), \rho_\downarrow(\mathbf{r})] d\mathbf{r}, \tag{24}$$

where $\varepsilon_{\mathrm{XC}}[\rho_\uparrow(\mathbf{r}), \rho_\downarrow(\mathbf{r})]$ is the exchange-correlation energy per an electron. The effective potential acting upon an ith electron by the rest of the many-electron ensemble is expressed as a functional derivative,

$$u_i(\mathbf{r}) = \frac{\delta E_{\mathrm{SIC}}}{\delta\rho_i(\mathbf{r})}. \tag{25}$$

The Kohn-Sham effective potential is the sum of the nuclear and electron components,

$$U(\mathbf{r}) = u_{\rm nucl}(\mathbf{r}) + u_i(\mathbf{r}). \tag{26}$$

The SIC can be applied to any density functional. In the present application, we used two different correlation-exchange functionals: the one proposed in Ref. 6 (GL76-SIC) and a simpler pure exchange functional (X-SIC).

The calculation of the one-electron orbitals $\varphi_i(\mathbf{r})$ and corresponding one-electro potentials $u_i(\mathbf{r})$ is carried out by the imaginary time evolution based on the solution of the equation

$$-\frac{\partial\varphi_i(\mathbf{r},t)}{\partial t} = \left[\frac{\hat{p}^2}{2} + u_{\rm nucl}(\mathbf{r}) + \alpha_k u_i(\mathbf{r})\right]\varphi_i(\mathbf{r},t). \tag{27}$$

The orthogonality to the occupied states is enforced on each step of the time evolution,

$$\varphi_i(\mathbf{r},t+0) = \varphi_i(\mathbf{r},t) - \sum_{j=1}^{i-1}\langle\varphi_j(\mathbf{r})|\varphi_i(\mathbf{r},t)\rangle\varphi_j(\mathbf{r}). \tag{28}$$

The stationary orbital is evaluated as the limit,

$$\varphi_i(\mathbf{r}) = \lim_{t\to\infty}\varphi_i(\mathbf{r},t) \tag{29}$$

After finding $\varphi_i(\mathbf{r})$, a new set of potentials $u_i(\mathbf{r})$ is determined and fed into Eq. (27) to start the next iteration. On the first iteration, the parameter $\alpha_1 = 0$, i.e., only the nuclear term is taken into account in Eq. (27). On the next iterations, $\alpha_{k>1}$ grows linearly with k reaching the value of $\alpha_{k>>1} = 1$. This way the inter-electron interaction is switched on gradually thus ensuring a smooth convergence of the solution.

The orbital energies are calculated as

$$\epsilon_i = -\frac{1}{2}\lim_{t\to\infty}\left[\frac{1}{\langle\varphi_i(\mathbf{r},t)|\varphi_i(\mathbf{r},t)\rangle}\frac{d\langle\varphi_i(\mathbf{r},t)|\varphi_i(\mathbf{r},t)\rangle}{dt}\right]. \tag{30}$$

Thus determined the ionization potential of the H_2 molecule is equal to $|\epsilon_1| = 16.1$ eV for X-SIC and 16.7 eV for GL76-SIC whereas the experimental value is 15.6 eV. The calculated ionization potentials $|\epsilon_i|$ of the H_2O molecule are shown in Table I in comparison with the experimental values from Ref. 7.

To solve the TDSE (13), we employed the one-electron effective potential $u_i(\mathbf{r})$ corresponding to the ground stationary state, and this potential was frozen during the whole ionization process (the frozen-core approximation).

C. Numerical implementation

In all the calculations, we assumed coincident polarization directions of XUV and IR fields, $\mathbf{n}_{\rm XUV} = \mathbf{n}_{\rm IR}$. The electron ejection direction was assumed collinear to the polarization direction, i.e., an electron momentum $\mathbf{k}_e \| \mathbf{n}_{\rm IR}$.

TABLE I. Calculated and experimental ionization potentials of the H_2O molecule.

Orbital	X-SIC	GL76-SIC	Experiment[7]
$1b_1$	11.6	12.3	12.6
$3a_1$	14.2	14.9	14.8
$1b_2$	17.5	18.3	18.7
$2a_1$	33.5	34.3	32.4

Below, we denote θ_e and ϕ_e as the polar and azimuthal angles that specify the direction of emission of an electron in a coordinate system tied to a molecule. The coordinate systems for H_2 and H_2O are shown in Fig. 1. The interatomic distances were assumed to coincide with the equilibrium positions, i.e., the distance between the hydrogen atoms in the hydrogen molecule was assumed to be 1.4 a.u., the distance between the oxygen atom and the hydrogen atoms in the water molecule was 1.811 a.u., and the angle between H atom was 104.45°.

A long IR pulse is modeled by a continuous wave with the frequency $\omega = 0.058\,41$ a.u. (photon energy 1.59 eV, $\lambda = 780$ nm) and the vector potential amplitude $A_{\rm IR} = 0.025$. The APT is modeled by a series of $N_{\rm APT} = 21$ with APT width $\tau_{\rm APT} = 2T_{\rm IR}$ (5.2 fs). The maximal amplitude of the XUV pulse was $A_{\rm XUV} = 0.025$ a.u.

The APT for H_2 is modeled by pulses with the width $\tau_{\rm XUV} = 1$ a.u. (24 as). Such a short pulse duration leads to a large spectral width and allows us to obtain the time delay results in a wide range of photoelectron energies. The central frequency was $\omega_{\rm XUV} = 29\omega$. The APT for H_2O is modeled by pulses with the width $\tau_{\rm XUV} = 2$ a.u. (48 as). The central frequency was $\omega_{\rm XUV} = 29\omega$.

By exposing an atom or a molecule to the APT with the central frequency $\omega_{\rm XUV} = (2q_0 + 1)\omega$, the photoelectrons will be emitted with the energies $E_{2q+1} = (2q + 1)\omega - E_0$ corresponding to the odd harmonics of the IR frequency ω. Superimposing a dressing IR field will add additional peaks in the photoelectron spectrum at $E_{2q} = 2q\omega - E_0$. These additional peaks, known as the sidebands (SBs), correspond to the even harmonics. The sideband amplitudes will vary with the relative time delay τ of the APT and the IR pulses as[8]

$$S_{2q}(\tau) = A + B\cos[2\omega(\tau - \tau_a)], \tag{31}$$

where τ_a is the atomic time delay. The atomic time delay can be written in a form

$$\tau_a = \tau_{\rm W} + \tau_{\rm CLC}\,, \tag{32}$$

where $\tau_{\rm W}$ is the Wigner time delay[9] and $\tau_{\rm CLC}$ is the Coulomb-laser coupling (CLC) correction.[10] Here we assume that there is no group delay (chirp) in the APT spectrum and all the harmonics have the same phase.

We solve the TDSE (13) using the orthogonal fast spherical Bessel transform as described in Ref. 11. In all the calculations, we set the box size to $\xi_{max} = 102.4$ a.u. The radial grid step was set to $\Delta\xi = 0.2$ a.u. The angular basis parameters were $N_\theta = 16$ and $N_\phi = 4$ for H_2, and $N_\theta = 4$ and $N_\phi = 6$ for H_2O. We tested the convergence of the calculated results

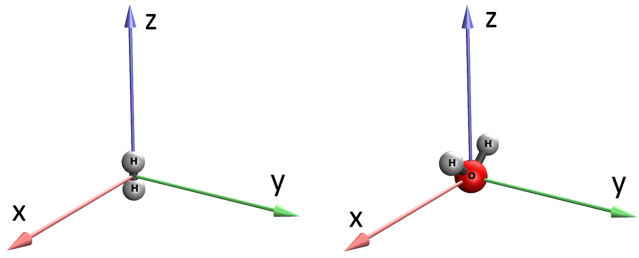

FIG. 1. Coordinate systems for H_2 and H_2O.

with the number of angular points both for the energies and time delays. The expansion of the coordinate grid starts at $t_1 = 0.25T_{IR} = 26.9$ a.u.

The relative APT/IR time delay τ was varied from 0 to $0.5T_{IR}$ with a step $0.031\,25T_{IR}$. The atomic time delay τ_a was obtained by fitting of the dependence of the magnitude of the SB on τ by the cosine curve Eq. (31) using the method of least squares.

To calculate the time delay for a non-aligned molecule, we numerically integrated the ionization differential cross section over the Euler angles (α, β, γ), which determines the orientation of the molecule with respect to the direction of polarization $\mathbf{n}_{IR}$. The number of angular grid points was $N_\alpha = 8$, $N_\beta = 4$, and $N_\gamma = 1$. A uniform grid was used for the angle α, and the Gauss-Legendre quadrature was used for the angle β. A single node was sufficient for the angle γ since we considered only the case $\mathbf{k}_e \| \mathbf{n}_{IR}$, and in this case, the differential cross section does not depend from the angle γ.

III. RESULTS

In Fig. 2, we display the atomic time delay of H_2 calculated by the TDCS method. Every energy point on the graph corresponds to a given SB. For comparison, another calculation is shown in which the Wigner time delay is calculated by the prolate spheroidal exterior complex scaling (PSECS),[12] and the CLC correction is introduced analytically.[13] The PSECS is an *ab initio* technique, and it returns the exact Wigner time delay for diatomic molecules. However, in the photoelectron energy range between 10 and 36 eV, the PSECS calculation on H_2 did not converge. Most likely, this is because of a large number of quasi-stationary states in this spectral range.

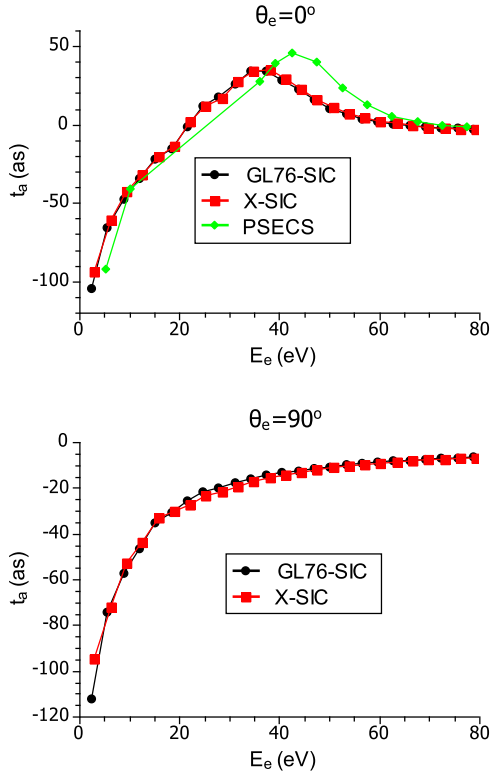

FIG. 2. Atomic time delay of H_2 as a function of the photoelectron energy E_e for emission in the polarization direction. The molecular axis is aligned along (top panel) and perpendicular (bottom panel) to the polarization direction.

The TDCS and PSECS + CLC results agree very well close to the threshold and are qualitatively similar at large excess energies. In the parallel molecular orientation, both set of calculations display a peak in the atomic time delay. However, in the TDCS calculation, this peak is shifted by 7 eV towards lower photoelectron energies (E_e = 35 eV in TDCS versus 42 eV in PSECS + CLC). Such a large difference can be explained by the poor performance of the DFT for such a few-electron systems such as H_2. We note that the peak displacement by 7 eV far exceeds an error of 1 eV in the ionization potential. This indicates that such a dynamic quantity as the atomic time delay is much more sensitive to inter-electron correlation than the static ionization potential.

On the other hand, the atomic time delay results, calculated with the help of the different density functionals (X-SIC and GL76-SIC), are very close each other, that is, a change in the effective potential caused by the introduction of correlation energy into the functional has almost no effect on the delay. Judging by this, it is hardly possible to improve the results of DFT for the time delay, remaining within the LDA framework. However, the apparent accuracy is sufficient to trust the results of our method for more complex targets such as the water molecule, especially for low energies, where the contribution of quasi-stationary states is absent.

Then, we calculated the atomic time delay in H_2O molecule corresponding to the ionization of the HOMO $1b_1$ and the HOMO-1 $3a_1$ (see Fig. 3). After the emission of the electron from the $1b_1$ orbitals, an ion is formed in the $\tilde{X}^+$ state, and after the emission of an electron from the $3a_1$ orbitals, an ion is formed in the $\tilde{A}^+$ state.

Various plotting symbols in Fig. 4 display the time delay for randomly oriented and aligned molecules. The aligned results correspond to photoelectron emission in the direction perpendicular to the nodal plane of the given orbital. In the case of $1b_1$, this plane contains the H atoms and the molecular dipole momentum vector. Therefore both perpendicular orientations produce identical results. The nodal plane of $3a_1$ is perpendicular to the dipole momentum and hence there are two distinctive perpendicular orientations: in the direction of the H atoms ($\theta = 0°$) and the reverse direction ($\theta = 180°$).

In the case of the $1b_1$ orbital, the randomly oriented time delay is nearly identical to the aligned results as the perpendicular emission is by far dominant. In the case of the $3a_1$ orbital, results are more complicated. At large photoelectron energies, the atomic time delay for $\theta = 180°$ is more negative than that

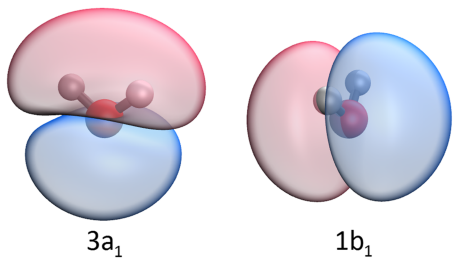

FIG. 3. The states of H_2O under consideration.

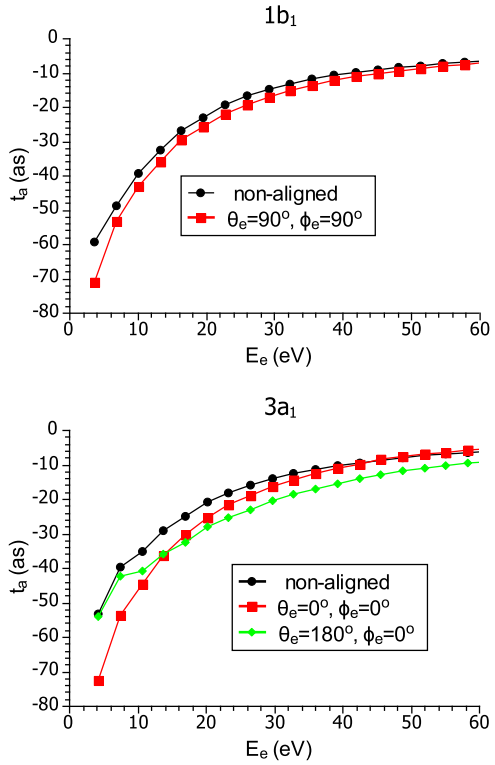

FIG. 4. Atomic time delay in H_2O for randomly oriented and aligned molecules. The top panel—the $1b_1$ orbital and the bottom panel—the $3a_1$ orbital.

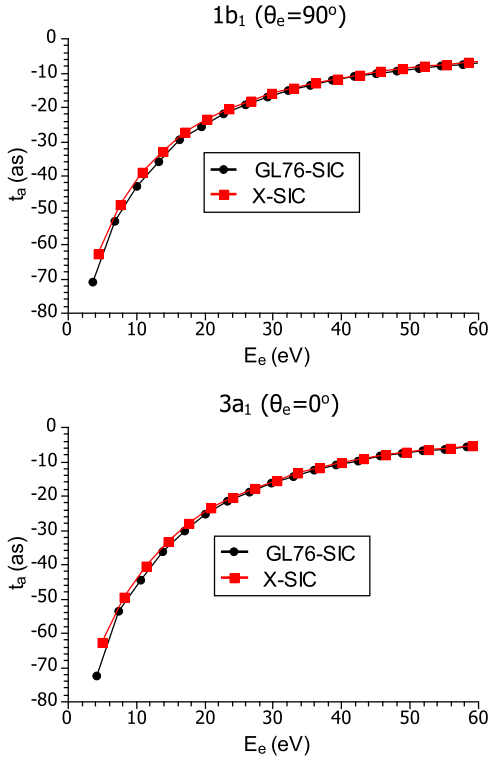

FIG. 6. Atomic time delays in H_2O calculated using GL76-SIC (circles) and X-SIC (rectangles) density functionals.

for $\theta = 0°$ which means the escape is faster in the O direction than in the H direction. However, this trend is reversed near threshold. Far away from the threshold, the non-aligned time delay is close to the one for $\theta = 0°$. Near the threshold, the non-aligned time delay is close to the one for $\theta = 180°$.

In Fig. 5, we display the time delay difference between the $3a_1$ and $1b_1$ orbitals at the same photon energy. It may seem surprising that the time delay difference is nearly vanishing in the whole studied energy range. This, however, may be explained by the fact that the randomly oriented water molecule may look like the neon atom and these two states in Ne differ only by the nodal plane orientation. In the same figure, we plot the experimental results by Huppert *et al.*[1] which

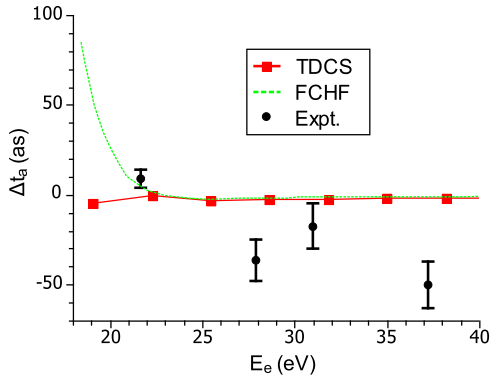

FIG. 5. Time delay difference between the $3a_1$ and $1b_1$ orbitals in the H_2O molecule as a function of the photon energy. The filled (red) squares—TDCS calculation, the (green) dashed line—the FCHF calculation,[1,2] and the filled black circles with error bars—experiment.[1]

show a sign variation of the time delay difference. The frozen-core Hartree–Fock (FCHF) calculation by the same authors Refs. 1 and 2 is also overplotted.

Both calculations are close to each other except for the very low photoelectron energy. Away from the threshold, both theories agree between each other, but their difference from the experimentally measured time delay exceeds a standard deviation. This disagreement between the two theories and the experiment may be due to the single active electron approximation adopted in both calculations. This approximation neglects the autoionizing states of the target molecule. The autoionizing states can strongly affect the measured time delay since the electron can remain in them long after the absorption of the photon before the electron is finally emitted from the molecule. The autoionizing states have been shown to affect the anisotropic time delay in the H_2 molecule.[14] It is known that the H_2O molecule has a number of autoionizing series in the energy range of interest.[15] The most suspicious one in the sense of influencing the experiment is a series resulting from excitation of an electron from the $2a_1$ orbital to a state above the HOMO. This series lies below the $2a_1$ ionization threshold of 32.4 eV.

Figure 6 shows that the choice of the exchange-correlation functional does not alter our results significantly. Even though the orbital energies are shifted for GL76-SIC relative to ones for X-SIC (Table I), the atomic time delays for both functionals lie on one curve.

IV. CONCLUSIONS

We combined the time-dependent coordinate scaling (TDCS) method, which we developed earlier for modeling of

RABBITT experiments,[3] with the density functional theory with self-interaction correction (DFT-SIC). An advantage of the TDCS method is the direct solution of the time-dependent Schrödinger equation driven by the superposition of the XUV and IR pulses without the splitting of the atomic time delay into the Wigner and CLC components. By using this technique, we calculated the photoionization time delay of the H_2 and H_2O molecules. In the case of H_2, we made a comparison with the *ab initio* PSECS calculations and found good agreement. In the case of H_2O, a comparison was made with experiment and agreement was found poor, but other theoretical methods such as FCHF did not perform any better.

The theory consistently points to nearly identical time delay from the HOMO and HOMO-1 orbitals of the randomly oriented water molecule. However, this time delay difference becomes noticeable on the oriented H_2O molecule. Hence, the experiments will be highly desirable in this oriented configuration which may reveal a reach and anisotropic ultrafast photoelectron dynamics. At the same time, the development of the theory beyond the single active electron approximation is necessary to account for autoionizing doubly excited states. These states have been shown to affect the anisotropic time delay in the H_2 molecule.[14]

[1] M. Huppert, I. Jordan, D. Baykusheva, A. von Conta, and H. J. Wörner, "Attosecond delays in molecular photoionization," Phys. Rev. Lett. **117**, 093001 (2016).
[2] D. Baykusheva and H. J. Wörner, "Theory of attosecond delays in molecular photoionization," J. Chem. Phys. **146**(12), 124306 (2017).
[3] V. V. Serov and A. S. Kheifets, "Angular anisotropy of time delay in XUV+IR photoionization of H_2^+," Phys. Rev. A **93**, 063417 (2016).
[4] V. V. Serov, V. L. Derbov, B. B. Joulakian, and S. I. Vinitsky, "Wave-packet-evolution approach for single and double ionization of two-electron systems by fast electrons," Phys. Rev. A **75**, 012715 (2007).
[5] J. P. Perdew and A. Zunger, "Self-interaction correction to density-functional approximations for many-electron systems," Phys. Rev. B **23**, 5048 (1981).
[6] O. Gunnarsson and B. I. Lundqvist, "Exchange and correlation in atoms, molecules, and solids by the spin-density-functional formalism," Phys. Rev. B **13**, 4274 (1976).
[7] C. Ning, B. Hajgató, Y. Huang, S. Zhang, K. Liu, Z. Luo, S. Knippenberg, J. Deng, and M. Deleuze, "High resolution electron momentum spectroscopy of the valence orbitals of water," Chem. Phys. **343**(1), 19 (2008).
[8] P. M. Paul, E. S. Toma, P. Breger, G. Mullot, F. Augé, P. Balcou, H. G. Muller, and P. Agostini, "Observation of a train of attosecond pulses from high harmonic generation," Science **292**(5522), 1689 (2001).
[9] E. P. Wigner, "Lower limit for the energy derivative of the scattering phase shift," Phys. Rev. **98**(1), 145 (1955).
[10] S. Nagele, R. Pazourek, J. Feist, K. Doblhoff-Dier, C. Lemell, K. Tőkési, and J. Burgdörfer, "Time-resolved photoemission by attosecond streaking: Extraction of time information," J. Phys. B: At., Mol. Opt. Phys. **44**(8), 081001 (2011).
[11] V. V. Serov, "Orthogonal fast spherical Bessel transform on uniform grid," Comput. Phys. Commun. **216**, 63 (2017).
[12] V. V. Serov, V. L. Derbov, and T. A. Sergeeva, "Interpretation of time delay in the ionization of two-center systems," Phys. Rev. A **87**, 063414 (2013).
[13] V. V. Serov, V. L. Derbov, and T. A. Sergeeva, "Interpretation of the time delay in the ionization of Coulomb systems by attosecond laser pulses," in *Advanced Lasers*, Volume 193 of Springer Series in Optical Sciences (Springer, Berlin, 2015), pp. 213–230.
[14] L. Cattaneo, J. Vos, R. Bello, A. Palacios, S. Heuser, L. Pedrelli, L. Gallmann, M. Lucchini, C. Cirelli, F. Martín *et al.*, "Nuclear-electronic coupled photoionization dynamics of H_2," in *14th International Conference On Multiphoton Processes* (Wigner Physics Research Center, Budapest, Hungary, 2017).
[15] M. Kato, T. Odagiri, K. Kodama, M. Murata, K. Kameta, and N. Kouchi, "Doubly excited states of water in the inner valence range," J. Phys. B: At., Mol. Opt. Phys. **37**, 3127–3148 (2004).